Chinese Chemical Letters 33 (2022) 4771–4775

Contents lists available at ScienceDirect

Chinese Chemical Letters

journal homepage: www.elsevier.com/locate/cclet

Graphene enhanced α-MnO_2 for photothermal catalytic decomposition of carcinogen formaldehyde

Xiaoshan Zeng, Chuanjia Shan, Mingdi Sun, Danni Ding, Shaopeng Rong*

Jiangsu Key Laboratory of Chemical Pollution Control and Resources Reuse, School of Environmental and Biological Engineering, Nanjing University of Science and Technology, Nanjing 210094, China

ARTICLE INFO

Article history:
Received 8 October 2021
Revised 30 November 2021
Accepted 30 December 2021
Available online 7 January 2022

Keywords:
α-MnO_2
Photothermal catalytic
Graphene oxide
Formaldehyde

ABSTRACT

Formaldehyde (HCHO) causes increasing concerns due to its ubiquitously found in indoor air and being irritative and carcinogenic to humans. Photothermal-catalysis developed in recent years has been considered as a significant strategy for enhancing catalytic activity. Manganese oxides, compared with its strong thermocatalytic activity, generally suffer from much lower photocatalytic activity make its photochemical properties less concerned. Herein, α-MnO_2 nanowires were composited with the graphene oxide (GO) *via* mechanical grinding and co-precipitating method, respectively. α-MnO_2/GO nanohybrids prepared by co-precipitating method exhibits excellent activity, achieving 100% decomposition of HCHO with the solar-light irradiation at ambient temperature. It is found that, besides the photo-driven thermocatalysis, the photocatalysis mechanism made a major contribution to the decomposition of HCHO. The incorporation of GO, on the one hand, is beneficial to improve the optical absorption capacity and photothermal conversion efficiency; on the other hand, is conductive to electron transfer and effective separation of electrons and holes. These synergistic effects significantly improve the catalytic activity of α-MnO_2/GO nanohybrids. This work proposes a new approach for the utilization of solar energy by combining manganese oxides, and also develops an efficient photothermal-catalyst to control HCHO pollution in indoor air.

Formaldehyde (HCHO), released from building and decoration materials, is one of the most common indoor air pollutants [1–3]. Due to the universality and carcinogenicity of HCHO, there is an urgent requirement for the elimination of indoor HCHO pollution. Therefore, various technologies, such as adsorption [4,5] and catalytic oxidation [6–13], have been developed for the elimination of HCHO in indoor air. Among many non-noble metal oxides, manganese dioxide (MnO_2) possesses much better catalytic activity at low-temperature [7–14]. By exposing high reactive facets [7], regulating the morphology [8,9], integrating anions or cations into lattice [10,11], and compositing with other materials [12,13], the catalytic activity of MnO_2 has been significantly improved. However, how to realize the complete decomposition of HCHO by non-noble metal catalysts at room temperature is still a great challenge. In recent years, photothermal-catalysis has been considered as a significant strategy for enhancing catalytic activity [15–21]. Li *et al.* [15] synthesized a nanoflower-like birnessite, which showed high catalytic efficiency in the irradiation of the visible-infrared light. Similarly, Dong's group [16] constructed a 3D-structured MS/PDA/MnO_x composite photothermocatalyst. It was found that the polydopamine (PDA) can efficiently absorb near infrared (NIR) radiation to heat the manganese oxides (MnO_x) catalyst, therefore initiating the oxidation of HCHO. Besides, they also assembled 2D layered MnO_x and GO into photothermocatalyst [17]. The superior photothermal effect of GO could rapidly increase the surface temperature of catalyst and then drive the thermocatalytic reaction of MnO_x. However, most of the previous literature attributed the improvement of catalytic activity to photo-driven thermocatalysis.

Generally, the photothermal-catalysis can be interpreted as three models: synergetic catalysis of photocatalysis and thermocatalysis; photo-driven thermocatalysis; thermally assisted photocatalysis. As to manganese oxides, many studies have attributed the enhancement mechanism to the photo-driven thermocatalysis. However, it is questionable that whether the catalytic process must be a photo-driven thermocatalysis mechanism. Manganese oxides, as a kind of semiconductor materials, are capable of photocatalytic activity in theory. Sasaki's group found that MnO_x nanosheets could generate the anodic photocurrent under visible light irradiation, suggesting that MnO_x may exhibit photocatalytic activity [22]. However, manganese oxides, compared with its strong

* Corresponding author.
E-mail address: rongrsp@njust.edu.cn (S. Rong).

https://doi.org/10.1016/j.cclet.2021.12.085
1001-8417/

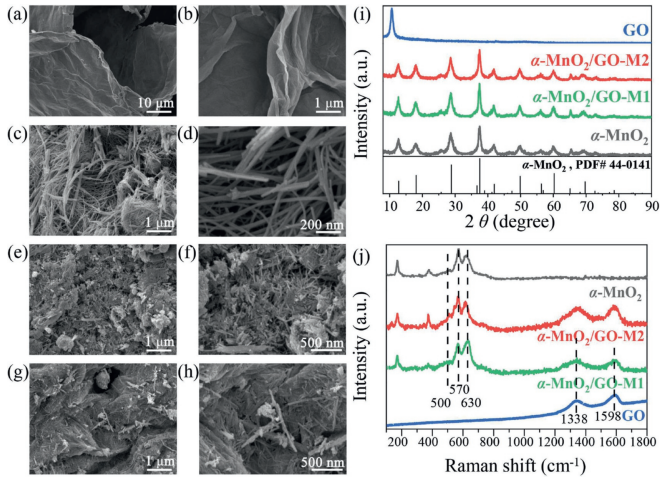

Fig. 1. SEM images of (a, b) GO, (c, d) α-MnO_2, (e, f) α-MnO_2/GO-M1 and (g, h) α-MnO_2/GO-M2. (i) The XRD pattern of different samples. (j) The Raman spectra of different samples.

thermocatalytic activity, generally suffer from much lower photocatalytic activity make its photochemical properties less concerned. Therefore, it is interesting to further study the photochemical properties and photothermal-catalysis mechanism of manganese oxides.

Previous literature has confirmed that graphene oxide (GO) has strong optical absorption and high photothermal conversion efficiency [17,23]. Therefore, it is possible to utilize GO to enhance the photothermal activity of MnO_x in the decomposition of HCHO. Herein, single-crystalline α-MnO_2 with predominantly exposed {310} facets were composited with GO *via* mechanical grinding and co-precipitating method, respectively. It was found for the first time that α-MnO_2 with exposed {310} facet exhibited excellent photocatalytic activity. The incorporation of GO could significantly enhance the photothermal effect of α-MnO_2. The α-MnO_2/GO nanohybrids prepared by co-precipitating method exhibited excellent activity, achieving 100% decomposition of HCHO with the solar-light irradiation at ambient temperature. The excellent catalytic activity of HCHO is mainly due to the synergetic effect of photocatalysis and photo-driven thermocatalysis.

In the experiment, the pristine α-MnO_2 was synthesized according to our previous publication [7]. Two facile approaches, namely mechanical grinding (α-MnO_2/GO-M1) and co-precipitating method (α-MnO_2/GO-M2), were applied to synthesize the nanohybrids of α-MnO_2 and GO. The specific preparation process was illustrated in the Supporting information.

The pristine α-MnO_2 nanowires were composited with GO *via* mechanical grinding and co-precipitating method, respectively. As shown in scanning electron microscope (SEM) images (Figs. 1a-h), α-MnO_2 exhibits the morphological characteristics of nanowires. Our previous study [7] has confirmed that the major exposure surface of α-MnO_2 is {310} facet. Moreover, two facile approaches, namely mechanical grinding (α-MnO_2/GO-M1) and co-precipitating method (α-MnO_2/GO-M2), were applied to synthesize the nanohybrids of MnO_2 and GO. As shown in the X-rays diffraction (XRD) patterns (Fig. 1i), all diffraction peaks of nanohybrids are indexed to pure α-MnO_2 (JCPDS, PDF #44–0141), which is a type of 2 × 2 tunnel structure with a size of about 4.6 Å. The diffraction peak at around 10° can be ascribed to characteristic diffraction peak of GO [24]. While the XRD of synthesized nanohybrids with two approaches are similar to each other, which all can be attributed to the α-MnO_2. After incorporating GO into α-MnO_2, there is no significant difference in the position and intensity of diffraction peaks between the nanohybrids and pristine α-MnO_2.

The SEM images of commercial GO and pristine α-MnO_2 show the morphology of sheet (Figs. 1a and b) and nanowire (Figs. 1c and d), respectively. When incorporating GO into α-MnO_2, there was a significant change in the macro morphology. In the SEM images of nanohybrids, both of the α-MnO_2 nanowires and GO nanosheets can be observed. Moreover, sub-micron GO sheets occupied the interspace of the interconnected network of α-MnO_2 nanowires, which allowed for better incorporation of α-MnO_2 and GO. By comparing these two nanohybrids prepared by mechanical grinding and co-precipitating method, it can be found that GO and α-MnO_2 in α-MnO_2/GO-M2 were mixed more evenly and combined more closely than that in α-MnO_2/GO-M1. As shown in Figs. 1e and f, the α-MnO_2/GO-M1 has poor encapsulation, and the loading of α-MnO_2 on the GO surface is rough and uneven. While as to the sample of α-MnO_2/GO-M2 (Figs. 1g and h), the coating of GO is better, and the loading of α-MnO_2 is more uniform. Compared with the mechanical grinding method, the co-precipitation after dispersion in the liquid phase is more conducive to the tight binding of nanoparticles. Obviously, the close contact between MnO_2 and GO facilitates to heat and electron transfer between these two materials [25,26].

Raman spectroscopy was also used to analyze the local structure of α-MnO_2 and GO (Fig. 1j). The major peaks at 1338 cm^{-1} and 1598 cm^{-1} can be attributed to the D and G band of GO. Moreover, the Raman bands located at around 500 cm^{-1}, 570 cm^{-1} and 630 cm^{-1} are typical spectra of MnO_2, which could be attributed to the stretching vibration of Mn-O-Mn, ν_3(Mn-O) stretching vibration caused by Mn^{4+} in the basal plane of the [MnO_6] sheet and the symmetric stretching vibrations (ν_2(Mn-O)), respectively [27]. In the spectra of nanohybrids samples, it can be clearly found that its Raman spectrum was just the superposition of α-MnO_2 and GO spectra.

To further figure out the surface chemical states, all samples were estimated by X-ray photoelectron spectroscopy (XPS). As shown in Fig. S1 (Supporting information), the spectrum of Mn $2p_{3/2}$ can be divided into two peaks, attributed to Mn^{3+} and Mn^{4+}, respectively. The molar atomic ratios of Mn^{3+}/Mn^{4+} for α-MnO_2, α-MnO_2/GO-M1, and α-MnO_2/GO-M2 are 0.78, 0.79, and 0.80, respectively. According to the binding energy difference of Mn 3s (Fig. S1b in Supporting information), the average oxidation state (AOS) of Mn was also calculated, and its results were listed in Table S1 (Supporting information). These results suggest that there is no significant difference in the valence distribution of Mn. Because the facile grinding and co-precipitation method obviously cannot significant change the chemical composition. Moreover, previous literature showed that once Mn^{3+} was present in MnO_2, oxygen vacancies would exist to maintain the charge balance [28]. When one oxygen vacancy is formed in MnO_2, two excess electrons are produced at the same time, which will result in reduction of two Mn^{4+} cations and formation of Mn^{3+} ions ($4Mn^{4+} + O^{2-} \rightarrow 2e^-/Vo + 4Mn^{4+} + 1/2O_2 \rightarrow Vo + 2Mn^{4+} + 2Mn^{3+} + 1/2O_2$, where Vo represents an oxygen vacancy in the lattice). It is widely accepted that the oxygen vacancy content is one of the significant factors affecting the catalytic activity. The O 1s spectra shown in Fig. S1c (Supporting information), can be divided into three peaks, namely 531.6–531.9 eV for surface residual water (O_{water}), 530.2–530.5 eV for surface adsorbed oxygen species (O_{ads}, such as O^-, O_2^-, and −OH group) and 528.7–529.1 eV for lattice oxygen (O_{latt}). Since oxygen and water molecules are widely exist in the atmosphere, they are more likely to be adsorbed at the surface oxygen vacancies and activated to produce surface-active oxygen species. These surface-active oxygen species tend to much higher activity and play a significant role in the HCHO catalytic oxidation at low temperature [29]. As displayed in Fig. S1d (Supporting

information), α-MnO_2/GO-M2 possesses the highest amount of O_{ads}, indicating that it may present the best activity in the decomposition of HCHO. α-MnO_2/GO-M2 nanohybrids were prepared by co-precipitating method, in which the GO and α-MnO_2 were dissolved in deionized water. On the one hand, dispersing in the liquid phase is beneficial to increase the surface-active oxygen species, especially the surface −OH. On the other hand, GO also has excellent adsorption properties, which can promote the adsorption of oxygen and water molecules. After incorporating GO into MnO_2, the content of O_{ads} in the nanohybrids become much higher than that in the pristine α-MnO_2.

The catalytic activity of HCHO oxidation was investigated by calculating the production of CO_2 in a fixed bed flow reactor equipped with a quartz glass window. As displayed in Fig. S2a (Supporting information), α-MnO_2/GO-M2–20% showed the highest catalytic activity, reaching 60% conversion of HCHO at room temperature under full-solar spectrum irradiation. In addition, it can be found that the conversion efficiency of HCHO decreased significantly with the introduction of GO reached to 50%. It is obvious that α-MnO_2 is the authentically active component in the decomposition of HCHO. When the content of α-MnO_2 in nanohybrids is reduced to a certain extent, the catalytic activity will be inhibited. For these two composite methods, when the doping ratio of GO to α-MnO_2 was 20%, they both exhibited better HCHO removal performance. Therefore, we chose a composite ratio of 20% for further experiments. It is worth noting that the catalytic activity of α-MnO_2/GO-M2–20% is better than that of α-MnO_2/GO-M1–20%, suggesting the composite method of co-precipitation is better than mechanical grinding. Just as mentioned before, co-precipitation makes the GO and α-MnO_2 mix more evenly and combine more closely, which is conducive to heat and electron transfer between these two substances. On the other hand, mechanical grinding may destroy the structure of large-area layered GO and produce more defects, which is not conducive to photon absorption and electron transfer. To confirm whether it is the solar-light radiation that caused improvement of catalytic efficiency, a set of parallel experiments under light-free conditions were conducted. Results showed that the conversion efficiency of all five catalysts decreased significantly under the dark condition (Fig. S2b in Supporting information). The comparison of catalytic activity with/without light irradiation confirms that full-spectrum illumination does improve the catalytic activity (Fig. S2c in Supporting information).

The effects of operating parameters on decomposition of HCHO, such as optical powers, space velocities and wavelength, were further investigated. Fig. 2a reflects the influence of optical power density on the catalytic activity. It can be found that the catalytic activity of α-MnO_2/GO-M2–20% is better than that of α-MnO_2/GO-M1–20% under the same optical power density. Moreover, the α-MnO_2/GO-M2 could reach complete conversion of HCHO at 250 mW/cm^2, while α-MnO_2/GO-M1 required 345 mW/cm^2. With the increase of optical power density, the performance of the catalyst is gradually enhanced. Obviously, higher optical power density can not only rapidly heat the catalyst and improve thermocatalytic activity, but also enhance the photocatalytic reaction process. Among many test conditions, the air flow speed has a significant impact on the catalytic performance. The effect of different gas hourly space velocity (GHSV) on the catalytic activity was also tested (Fig. 2b). At ambient temperature with low airspeed (GHSV = 120 L g^{-1} h^{-1}), both α-MnO_2/GO-M1 and α-MnO_2/GO-M2 could achieve complete conversion of HCHO. However, with the airspeed increased, the conversion efficiency of both nanohybrids decreased significantly. Herein, it should be noted that, even under more stringent test conditions, the catalytic activity of α-MnO_2/GO-M2–20% is still better than that of α-MnO_2/GO-M1–20%.

In order to investigate the influence of wavelength on the photocatalytic process, the activities of two nanohybrids equipped with different wavelength cutoff filters were tested. As shown in Figs. 2c and d, with the light is continuously filtered, the catalytic activity shows a downward trend. When wavelengths >630 nm, the conversion efficiency of α-MnO_2/GO-M1 drops to 34.9% and α-MnO_2/GO-M2 to 40.5%, respectively. Moreover, it can be found that α-MnO_2 shows relatively high activity in ultraviolet and visible region, but relatively low catalytic activity in infrared region. Finally, the stability of two nanohybrids was also evaluated. As displayed in Fig. S3 (Supporting information), the HCHO conversion in nanohybrids remained stable at 100% within 12 h test periods, indicating its long-term photothermal catalytic stability.

Solar-light radiation will bring two significant effects, one is the thermal effect and the other is the photoactivity. Until now, the definition of photothermal-catalysis is still vague. It can be interpreted as three models: synergetic catalysis of photocatalysis and thermocatalysis; photo-driven thermocatalysis; thermally assisted photocatalysis. The nanohybrids of α-MnO_2/GO exhibited excellent catalytic activity for HCHO decomposition under solar-light irradiation at room temperature. Therefore, it is necessary and meaningful to investigate the mechanism of catalytic reaction. The high conversion efficiency exhibited by α-MnO_2/GO under Xenon lamp irradiation may be triggered by the following two mechanisms. One is the photo-driven thermocatalysis, and the other is conventional photocatalysis mechanism. According to the study on carbon-based manganese dioxide composites [30], we initially believed that the increase in the conversion efficiency of HCHO was due to the photo-driven thermocatalysis. Obviously, the surface temperature of the catalyst will rise rapidly under the continuous irradiation of solar-light. As shown in Fig. S4 (Supporting information), under full-solar spectrum irradiation, the equilibrium temperature of α-MnO_2/GO-M1 and α-MnO_2/GO-M2 were 28 °C and 31 °C, respectively. Nevertheless, the stabilization temperature of the nanohybrids was still steadily higher than that of the pristine α-MnO_2. The increase of temperature can be attributed to the heating effect generated from the quick non-radiative recombination of the electron-hole pairs produced by the d-d transitions of Mn ions upon the absorption of photons [15]. As for GO, because of the strong absorption of NIR, the temperature reached to about 28 °C. Besides, the surface temperature of GO with light radiation is also higher than that of α-MnO_2 (Fig. S4 in Supporting information). When GO was incorporated into α-MnO_2, the temperature reached as high as about 31 °C, even higher than that of GO. It can be attributed to the excellent thermal conductivity of GO, resulting in the higher equilibrium temperature. Therefore, nanohybrids of α-MnO_2 and GO could fully absorb solar spectra and also efficiently transfer heat energy to α-MnO_2 for HCHO oxidation.

However, in this case, unlike previous carbon-based manganese dioxide composites [30], the photothermal effect was not significant for the nonhybrids prepared in this research. To further investigate the surface temperature variation, we tested the surface equilibrium temperature of the nanohybrids at the wavelengths of full-spectrum, >400, >470, >550, and >630 nm. The optical power densities of α-MnO_2/GO-M1 and α-MnO_2/GO-M2 were controlled at 345 mW/cm^2 and 250 mW/cm^2, respectively. As displayed in Fig. S5 (Supporting information), the increase of surface temperature was insignificant, and the final equilibrium temperature was much lower than that required for conventional thermal catalysis. What else, simply heating the catalysts to this equilibrium temperature range does not enable the complete conversion of HCHO. Herein, it should be pointed out that, under solar-light irradiation, photo-driven thermocatalytic mechanism also contributes to the removal performance, but it's not exactly the case. As to the α-MnO_2/GO-M2, it can completely convert HCHO into CO_2 with the irradiation of solar-light at the optical power densities of 250 mW/cm^2. While at the same light conditions, the heating temperature driven by light irradiation cannot reach the complete

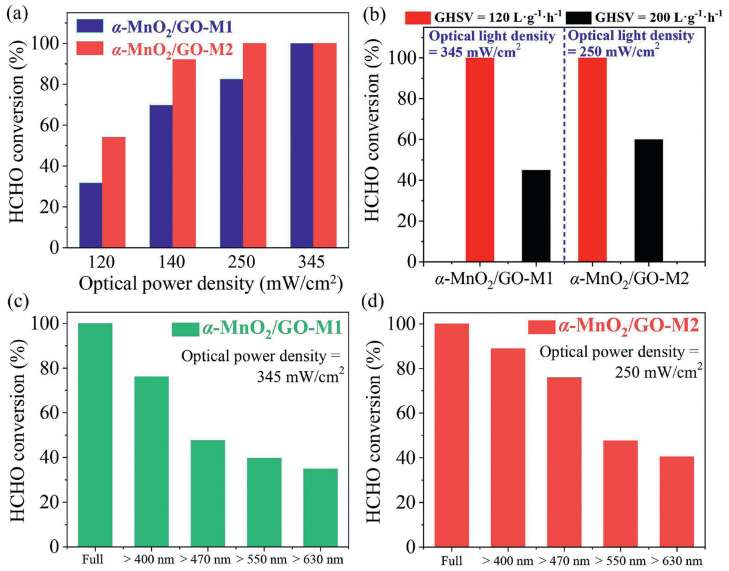

Fig. 2. (a) The effect of optical power density on the HCHO conversion; (b) the effect of GHSV on the HCHO conversion; the effect of wavelength on the HCHO conversion: (c) α-MnO_2/GO-M1 and (d) α-MnO_2/GO-M2.

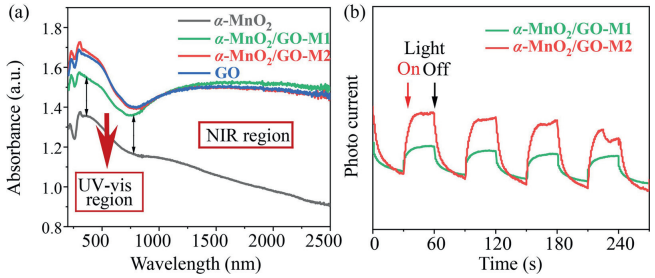

Fig. 3. (a) UV–vis-NIR diffuse reflectance spectrum and (b) the photocurrent response.

decomposition of HCHO. Therefore, besides the photo-driven thermocatalytic mechanism, the photocatalytic mechanism may be the main reason for the decomposition of HCHO.

Manganese dioxides, as a kind of semiconductor materials, are capable of photocatalytic activity in theory. Photocatalyst should respond to wide-range light, so that it may be able to absorb photon energy of multiple wavelengths, generate more photogenerated electron-hole pairs, and thereby further oxidize pollutants. To reveal the mechanism, the light responses of different samples were recorded by the diffuse reflectance UV–vis-NIR spectra (Fig. 3a). The result shows that α-MnO_2 has strong absorption for UV–vis light, but when the wavelength of light is above 760 nm, its absorbance decreases significantly. It is worth noting that GO has non-selective absorption for the full spectrum, especially for visible light [31]. After GO was compounded with MnO_2, the light-absorbance of α-MnO_2/GO-M1 and α-MnO_2/GO-M2 increased significantly, especially for the vis-IR section. In addition, according to Tauc plot converted from diffuse reflectance spectra, the band-gap energy (E_g) of the three samples were also measured. As shown in Fig. S6 (Supporting information), the E_g of the α-MnO_2, α-MnO_2/GO-M1 and α-MnO_2/GO-M2 are estimated to be 1.51 eV, 1.47 eV and 1.45 eV respectively. Therefore, it can be confirmed that GO is not only beneficial to enhance the photoabsorption capacity of α-MnO_2, but also helps to reduce the band gap of the nanohybrids.

As a photocatalysts, its photocurrent reflects the photoelectric efficiency, and indirectly determines the photocatalysis activity. Fig. 3b shows the photocurrent response of nanohybrids under full-spectrum illumination. When the light is turned on, both nanohybrids generate a constant photocurrent intensity. Moreover, the detection of photocurrent also directly proved the possibility of photocatalytic activity in α-MnO_2/GO. It is further confirmed that the elimination of HCHO with irradiation of solar-light on α-MnO_2/GO is consistent with photocatalytic process. Compared with the α-MnO_2/GO-M1, α-MnO_2/GO-M2 generated a stronger photocurrent. It implies that α-MnO_2/GO-M2 is more effective for the separation of photogenerated electron-hole pairs and owns a longer lifetime of photogenerated charge carriers. When the Xenon lamp shines down, α-MnO_2/GO is irradiated with solar-light which is greater than the bandgap energy, where electrons in the valence band (VB) jump to the conduction band (CB). Subsequently, photogenerated electrons (e^-) are produced in the conduction band, while photogenerated holes (h^+) are produced in the valence band [32]. Then the electrons and holes are combined with the oxygen and water adsorbed on the surface of the catalyst to form $^{\bullet}O_2^-$ and $^{\bullet}OH$. Finally, these highly active or oxidizing radicals can decompose and mineralize HCHO adsorbed on the surface of the catalyst. As exhibited in EPR (electron paramagnetic resonance) (Fig. S7 in Supporting information), $^{\bullet}O_2^-$ is detected on α-MnO_2 even without the solar-light irradiation, whose phenomenon has also been confirmed by other literature [9,30]. When α-MnO_2 was irradiated by Xenon lamp, much higher intensity of $^{\bullet}O_2^-$ EPR signal was observed compared to that under dark condition. It indicates that solar-light irradiation promotes the production of $^{\bullet}O_2^-$ in the surface of α-MnO_2. Interestingly, besides the $^{\bullet}O_2^-$, the additional weak signal of $^{\bullet}OH$ was also detected with the solar-light irradiation. Photogenerated holes with strong oxidation ability, which can oxidize H_2O or $-OH$ and produce $^{\bullet}OH$. The detection of $^{\bullet}OH$ with solar-light irradiation also indirectly proved that the photocatalytic reaction did take place on the surface of α-MnO_2. In pristine MnO_2, most of the photogenerated electron-hole pairs recombine and disappear, thus revealing a poor photocatalytic activity. However, the introduction of GO effectively promotes the separation of electron-hole pairs [33,34]. On the one hand, due to the excellent electrical conductivity and unique two-dimensional layered structure, GO can increase the migration rate of photogenerated electrons, reduce the recombination of photogenerated electrons and holes, and improve the quantum efficiency of photocatalysis [33–35]. On the other hand, GO, as a carbon-based material with special structure, has a certain adsorption capacity for HCHO [36]. In the special structure of MnO_2/GO, HCHO can be adsorbed

to the catalyst surface due to the adsorption of GO. But it should be noted that the contribution of adsorption is negligible compared with photocatalysis and thermal decomposition. Obviously, HCHO cannot be decomposed into CO_2 by adsorption alone.

In summary, the nanohybrids of MnO_2 and GO were synthesized *via* mechanical grinding and co-precipitating method, respectively. With solar-light irradiation, the nanohybrids of α-MnO_2/GO exhibited excellent catalytic activity for HCHO decomposition at room temperature. In general, the α-MnO_2/GO-M2–20% prepared by co-precipitating method shows the best catalytic activity for the oxidation of HCHO, which could completely transform HCHO into CO_2. Compared with the mechanical grinding method, the co-precipitation method is more conducive to the tight binding of nanoparticles. It is confirmed that GO can significantly enhance the photothermal effect of α-MnO_2, and further enhance decomposing of HCHO at ambient temperature. The incorporation of GO, on the one hand, is beneficial to improve the optical absorption capacity and photothermal conversion efficiency; on the other hand, is conductive to electron transfer and effective separation of electrons and holes. Besides the photo-driven thermocatalysis, the photocatalysis mechanism makes a major contribution to the decomposition of HCHO. This work offers a new strategy for the utilization of solar energy by combining catalyst with photothermal material, and also extends the research of manganese oxides on photocatalysis.

Declaration of competing interest

The authors declare that they have no known competing financial interests or personal relationships that could have appeared to influence the work reported in this paper.

Acknowledgments

This work was financially supported by National Natural Science Foundation of China (No. 21906084) and the National Undergraduate Training Program for Innovation and Entrepreneurship (No. 202010288026Z).

Supplementary materials

Supplementary material associated with this article can be found, in the online version, at doi:10.1016/j.cclet.2021.12.085.

References

[1] R. Atkinson, J. Arey, Atmos. Environ. 2 (2003) 197–219.
[2] C. Jiang, D. Li, P Zhang, et al., Build. Environ. 117 (2017) 118–126.
[3] X. Tang, Y. Bai, A. Duong, et al., Environ. Int. 35 (2009) 1210–1224.
[4] J. Bellat, I. Bezverkhyy, G. Weber, et al., J. Hazard. Mater. 300 (2015) 711–717.
[5] L. Wang, X. Liang, Z. Chang, et al., ACS Appl. Mater. Interfaces 10 (2018) 42–46.
[6] X. Yu, J. He, D. Wang, et al., J. Phys. Chem. B 116 (2012) 851–860.
[7] S. Rong, P. Zhang, F. Liu, Y. Yang, ACS Catal. 8 (2018) 3435–3446.
[8] T. Chen, H. Dou, X. Li, et al., Micropor. Mesopor. Mat. 122 (2009) 270–274.
[9] T. He, D. Shao, X. Zeng, S. Rong, Chemosphere 261 (2020) 127778.
[10] T. He, X. Zeng, S. Rong, J. Mater. Chem. A 8 (2020) 8383–8396.
[11] J. Wang, D. Li, P. Li, et al., RSC Adv. 122 (2015) 100434–100442.
[12] Y. Sekine, A. Nishimura, Atmos. Environ. 35 (2001) 2001–2007.
[13] S. Rong, P. Zhang, J. Wang, et al., Chem. Eng. J. 306 (2016) 1172–1179.
[14] J. Ma, R. Cao, Y. Dang, J. Wang, Chin. Chem. Lett. 32 (2021) 2985–2993.
[15] F. Liu, M. Zeng, Y. Li, et al., Adv. Funct. Mater. 26 (2016) 4518–4526.
[16] Z. Wang, H. Yu, Y. Xiao, et al., J. Hazard. Mater. 407 (2021) 124795.
[17] Z. Wang, H. Yu, Y. Xiao, et al., Chem. Eng. J. 394 (2020) 125014.
[18] E. Yi, J. Li, J. Chen, et al., J. Hazard. Mater. 388 (2020) 121800.
[19] E. Yi, J. Li, H. Jia, J. Hazard. Mater. 399 (2020) 122942.
[20] M. Zhang, S. Cai, J. Li, et al., J. Hazard. Mater. 412 (2021) 125266.
[21] J. Li, M. Zhang, E. Elimian, et al., Chem. Eng. J. 412 (2021) 128560.
[22] N. Sakai, Y. Ebina, K. Takada, T. Sasake, J. Phys. Chem. B 109 (2005) 9651–9655.
[23] J. Liang, Y. Xu, Y. Huang, et al., J. Phys. Chem. C 113 (2009) 9921–9927.
[24] B. Paulchamy, G. Arthi, B.D. Lignesh, J. Nanomed. Nanotechnol. 6 (2015) 1000253.
[25] J. Li, S. Cai, E. Yu, et al., Appl. Catal. B: Environ. 233 (2018) 260–271.
[26] J. Li, S. Cai, Chen X, et al., J. Mater. Chem. A 7 (2019) 11985–11995.
[27] M. Polverejan, J. Villegas, S.L. Suib, J. Am. Chem. Soc. 126 (2004) 7774–7775.
[28] X. Liu, K. Zhou, L. Wang, B. Wang, Y. Li, J. Am. Chem. Soc. 131 (2009) 3140–3141.
[29] B. Chen, B. Wu, L. Yu, M. Crocker, C. Shi, ACS Catal. 10 (2020) 6176–6187.
[30] J. Wang, G. Zhang, P. Zhang, Appl. Catal. B: Environ. 349 (2018) 77–85.
[31] Z. Shayegan, C. Lee, F. Haghighat, Chem. Eng. J. 375 (2019) 533–546.
[32] I. Khan, M. Sadiq, I. Khan, K. Saeek, Environ. Sci. Pollut. Res. 26 (2019) 5140–5154.
[33] E. Castro, K. Novoselov, S. Morozov, et al., Phys. Rev. Lett. 99 (2007) 216802.
[34] C. Gómez-Navarro, R. Weitz, A. Bittner, et al., Nano Lett. 7 (2007) 3499–3503.
[35] T. Nguyen-Phan, V. Pham, E. Shin, et al., Chem. Eng. J. 170 (2011) 226–232.
[36] H. Tan, D. Chen, N. Li, et al., Chem. Eur. J. 25 (2019) 16718–16724.